ADVANCED THERAPEUTICS
www.advtherap.com

Development of Innovative Antiatherosclerotic Peptides through the Combination of Molecular Modeling and a Dual (Biochemical-Cellular) Screening System

*Aleyda Benitez-Amaro, Chiara Pallara, Laura Nasarre, Ruben Ferreira, David de Gonzalo-Calvo, Roger Prades, Teresa Tarragó, and Vicenta Llorente-Cortés**

Cardiovascular disease (CVD) is a leading cause of death worldwide. Approximately 60% of patients treated with low-density lipoprotein (LDL)-lowering drug treatments, with on-target plasma cholesterol levels, are still suffering clinical acute ischemic events. Mechanisms, such as LDL aggregation, underlie extracellular and intracellular cholesterol accumulation in the vasculature. A peptide sequence (P3) of the low-density lipoprotein receptor-related protein 1 (LRP1) efficiently protects LDL from sphingomyelinase (SMase-) and phospholipase A2 (PLA_2)-induced LDL aggregation. The aim is to design families of peptide derivatives from P3 with enhanced potency and proteolytic stability. New peptides are designed through in silico conformational sampling and ApoB-100 molecular docking, and are tested in dual (biochemical-cellular) screening assays. A total of 46 new peptides including linear, fragment, cyclic, and alanine scanning derivatives are generated through two consecutive optimization rounds. Structurally and functionally optimized peptides contain hotspot residues that are replaced by alanine. This strategy confers an increased capacity to form prone alpha-helix conformations crucial for the electrostatic interaction with ApoB-100. These new compounds are highly efficient at inhibiting LDL aggregation and human coronary vascular smooth muscle cell-cholesteryl ester loading and should be studied in preclinical models of atherosclerosis.

1. Introduction

Ischemic heart disease is the primary cause of death in Western countries, and myocardial infarction accounts for ≈50% of deaths from this disease. The Framingham study showed that cardiovascular risk positively correlates with low-density lipoprotein (LDL)-cholesterol and inversely with high-density lipoprotein (HDL)-cholesterol.[1,2] High levels of LDL-cholesterol induce alterations in the endothelium permeability, which in turn promote LDL influx into the arterial intima.[3] Intimal LDL-cholesterol accumulation is a critical step in vascular cholesteryl ester (CE) deposition, a process that increases the tendency of the atherosclerotic plaque to rupture, triggering thrombosis and the development of ischemic cardiomyopathy.[4–6] Cholesteryl esters in atherosclerotic plaques are deposited both extra- and intracellularly. Extracellular deposition of LDL-CEs, a central initiating event in atherosclerosis, is mediated by proteoglycans in the extracellular matrix of the arterial intima. The electrostatic interaction between proteoglycans

A. Benitez-Amaro, L. Nasarre, Dr. D. de Gonzalo-Calvo, Dr. V. Llorente-Cortés
Institute of Biomedical Research of Barcelona (IIBB)
Spanish National Research Council (CSIC)
Barcelona 08036, Spain
E-mail: vicenta.llorente@iibb.csic.es; Cllorente@santpau.cat

The ORCID identification number(s) for the author(s) of this article can be found under https://doi.org/10.1002/adtp.202000037

DOI: 10.1002/adtp.202000037

A. Benitez-Amaro, Dr. D. de Gonzalo-Calvo, Dr. V. Llorente-Cortés
Group of Lipids and Cardiovascular Pathology
Biomedical Research Institute Sant Pau (IIB Sant Pau)
Hospital de la Santa Creu i Sant Pau
Barcelona 08025, Spain

Dr. C. Pallara, Dr. R. Ferreira, Dr. R. Prades, Dr. T. Tarragó
Iproteos S.L
Barcelona Science Park (PCB)
Barcelona 08028, Spain

Dr. D. de Gonzalo-Calvo, Dr. V. Llorente-Cortés
CIBER enfermedades cardiovasculares (CIBER*cv*)
Madrid 28029, Spain

and LDL and the proteolytic/lipolytic actions of enzymes on LDL are enhanced in the arterial intima and promote LDL retention and aggregation.[7,8] Two of the main enzymes that act on intimal retained LDL and play key roles in LDL aggregation in the arterial intima during atherogenesis are sphingomyelinase (SMase) and phospholipase A_2 (PLA_2).[9–12] Aggregated LDL (agLDL) has been detected and isolated from atherosclerotic plaques from animal models and humans.[10,13] Unlike native LDL, agLDL is a potent inducer of massive intracellular CE accumulation both in macrophages and human coronary vascular smooth muscle cells (hcVSMCs).[14–18] In hcVSMCs, we reported that agLDL is actively taken up through the low-density lipoprotein receptor-related protein 1 (LRP1) which, in turn, induces LRP1 expression, promoting a positive feedback loop that efficiently transforms hcVSMCs into foam cells.[19,20] hcVSMC-foam cells synthesize and release high amounts of tissue factor, which is crucial for the prothrombotic transformation of the vascular wall and thus for the progression of atherosclerosis to thrombosis.[21,22] The relevance of this mechanism in atherosclerosis is evident since vascular smooth muscle cells (VSMCs) are the main component of the vascular wall and more than 50% of foam cells previously considered to be monocyte-derived macrophages in human atherosclerotic plaques originate from VSMCs.[23] Together, these findings support the notion that the generation of hcVSMC-derived foam cells through LRP1-mediated agLDL uptake is a key mechanism underlying cholesterol accumulation in vasculature susceptible to atherosclerosis. Our group has identified LRP1 cluster II, in particular the region Gly^{1127}-Cys^{1140} (peptide LP3: H_2N-GDNDSEDNSDEENC-NH_2) that spans the *C*-terminal half of domain CR9, as pivotal for binding to agLDL and subsequent internalization of agLDL into human VSMCs.[24] Moreover, we have shown that anti-LP3 antibodies reduce high fat diet-induced atherosclerosis in a rabbit model.[25] In addition, we have shown that LRP1-derived peptides (the original LP3 and its retroenantiomer version-DP3) are protective against LDL aggregation, even in conditions of extreme lipolysis due to the maintenance of ApoB-100 conformation.[26] We showed that DP3 forms a complex with ApoB-100 and this molecular interaction stabilizes ApoB-100 conformation. ApoB-100 conformation stabilization might guarantee the structural preservation of surface cholesterol-enriched environments, where sphingomyelin (SM) is located. Structural preservation of cholesterol, a key regulator of phospholipolysis, would protect SM from SMase activity. As a result, LDL complexed with DP3 remains unaltered when exposed to SMase. This scenario changes when LDL complexed with DP3 is exposed to PLA_2. The target for PLA_2 is phosphatidylcholine (PC), a phospholipid associated with low-cholesterol environments. Therefore, PC is unprotected against the attack of PLA_2, which hydrolyses PC producing lysoPC and nonesterified fatty acids. Remarkably, LDL complexed with DP3 is protected against SMase and PLA_2-induced aggregation even in conditions of extreme phospholipolysis, indicating that the maintenance of ApoB-100 conformation is enough to prevent LDL aggregation.

The main objective of the present study is to design and evaluate a series of antiatherosclerotic families of peptides with potential for in vivo application.

Table 1. Parameters for validation of biochemical (SMase-TB and PLA_2-TB) and cell-based (SMase-CE/FC) assays. These parameters were obtained from the mean and SD of the values obtained with positive (DP3) and negative control (P321) in ten different experiments performed by quatriplicate (SMase-TB assay) or duplicate (PLA_2-TB and SMase-CE/FC ratio assays). SMase: Sphingomyelinase; PLA_2: phospholipase A_2; TB: turbidimetry; CE: cholesteryl esters; FC: free cholesterol.

	SMase-TB	PLA_2-TB	SMase-CE/FC
CV interassay [%]	11.60	7.97	12.79
CV intra-assay [%]	6.24	6.32	8.47
Estimated Z-factor	0.86	0.60	0.75

2. Results

2.1. Feasibility of Biochemical and Cell-Based Assays for Compound Screening

The scheme of the biochemical SMase and PLA_2-induced LDL turbidimetry (SMase-TB and PLA_2-TB assays) and cell-based assays (SMase-CE/free cholesterol (FC) assay) is described in Figure S1 of the Supporting Information. The potential of these assays as screening tools was evaluated by calculating the intra-assay and interassay coefficient of variation (CV) using a positive (DP3) and a negative control (P321) through several experiments performed in quadruplicate (SMase-TB) or duplicate (PLA_2-TB and SMase-CE/FC) (Figure S2, Supporting Information). As shown in **Table 1**, the assays have an interassay CV < 15% and an intra-assay CV < 10%, showing the robustness of the assays and their feasibility to be used as evaluation tools. In addition, we calculated the Z-factor, a pivotal parameter for comparison and evaluation of the quality of the assays that reflects both the assay signal dynamic range and the data variation associated with the signal measurements and therefore suitable for assay quality assessment.[27] The calculated Z-factor for the three assays was between 0.5 and 1.0 (Table 1), indicating the suitability of these assays for screening of the effect of compounds on LDL aggregation and foam cell formation.

2.2. Computational Design and Screening of Peptides from the First-Round Optimization

2.2.1. Computational Peptide Design

The computational approach used to design optimized peptides yielded 20 exploratory compounds that were produced by solid-phase peptide synthesis (summarized in **Figure 1**). The characterization and sequence of designed peptides have been detailed in Tables S1 and S2 of the Supporting Information, respectively.

Considering the lack of structural information about the LRP1 receptor, the ApoB-100 protein and the low reliability of the corresponding homology models currently available, the computational design of CR9-based peptide analogues was performed by combining a ligand-based method that completely neglects receptor 3D information and relies only on the physicochemical

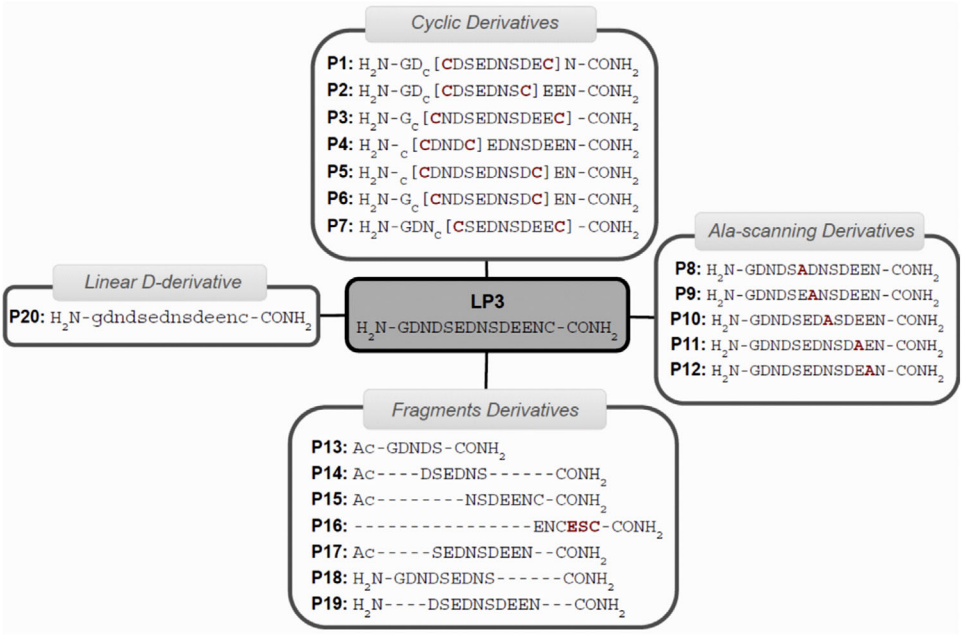

Figure 1. Schematic representation of the designed peptide groups through the development of the first-round optimization. Ala: Alanine.

and dynamic properties of the ligands, with a structure-based protocol, based on molecular docking approach.

The first molecular strategy was based on the hypothesis that unbound biomolecules (i.e., proteins, nucleic acids, peptides, small molecules) naturally adopt a variety of conformational states, a subset of which are suitable to bind to their biological partner.[28,29] An exhaustive conformational sampling of the LP3 peptide was performed by molecular dynamics (MD) simulations. The most populated low energy states were extracted, considered to the ones most similar to the bound state, and then, if possible, conformationally restricted in cyclic analogues by mutating two specific residues to cysteine, chosen as the most suitable residues for creating rigid rings with relatively low synthetic complexity. Finally, this strategy led to six cyclic analogues mimicking low-energy near-native bound conformations of LP3 peptide, namely peptides P1, P2, P3, P4, P5, and P6.

The second computational protocol emerged from the idea that interacting partners that are involved in initial encounters evolve toward the final specific complex by mutually adjusting their interfaces.[30] In accordance to this, multiple molecular docking simulations were performed taking into account several alternative conformations of both the receptor and the ligand, namely, ApoB-100 protein and LP3 peptide, respectively. Then, the most favorable docking complex was submitted to molecular dynamic simulations in order to favor the mutual adjustment of the docking partners and explore active-like conformations of the peptide. The most LP3 active-like conformation was conformationally restricted in a cyclic analogue that was named P7 peptide.

An additional 13 LP3 derivatives were designed based on the careful evaluation of the final docking complexes, as described below. The objective was to obtain a better understanding of the mechanism of interaction between the original CR9 domain peptide and ApoB-100 protein. Although the protein–protein binding interface involved many contacts distributed throughout the entire surface, it is known that in many cases only a small subset of individual amino acids, the so-called hotspots, contribute the most to the free energy of binding.[31] Homology modeling and molecular dynamics methods combined with molecular docking provided the structural model of LP3 peptide in complex with ApoB-100 and offered a detailed insight into the mechanistic basis of LP3 recognition by ApoB-100 protein.[26] Moreover, this result facilitated the identification of several specific residues (namely Glu^6, Asp^7, and Asp^{10}) found to be deeply buried upon binding. To confirm the key role of these residues, the suspected hotspot residues in the P17 sequence were replaced by alanine residues because of its small and nonreactive side chain, thus obtaining several LP3 alanine scanning analogue peptides (P8, P9, P10, P11, and P12).

Shorter peptide sequences, derived from the parent peptide (LP3) were also analyzed. These peptides (P13, P14, P15, P16, P17, P18, and P19) were useful to identify the minimal peptide sequence length responsible for the inhibitory activity of LDL aggregation.

Finally, the enantiomer version of LP3 peptide was explored (P20 peptide), with an expectation of a lower inhibitory activity against LDL aggregation but on the other hand a theoretical enhanced plasma stability given by the high proteolytic resistance of D-amino acids containing peptides.[32]

2.2.2. Peptide Screening

SMase-TB: The inhibitory effect of these exploratory compounds on SMase-induced LDL aggregation is shown in **Figure** 2A. Surprisingly, P20 peptide, the enantiomer version of LP3, displayed similar activity compared to the original peptide, which is encouraging given its expected higher plasma stability compared to the LP3 peptide (all L-amino acids). Additionally, three out of seven

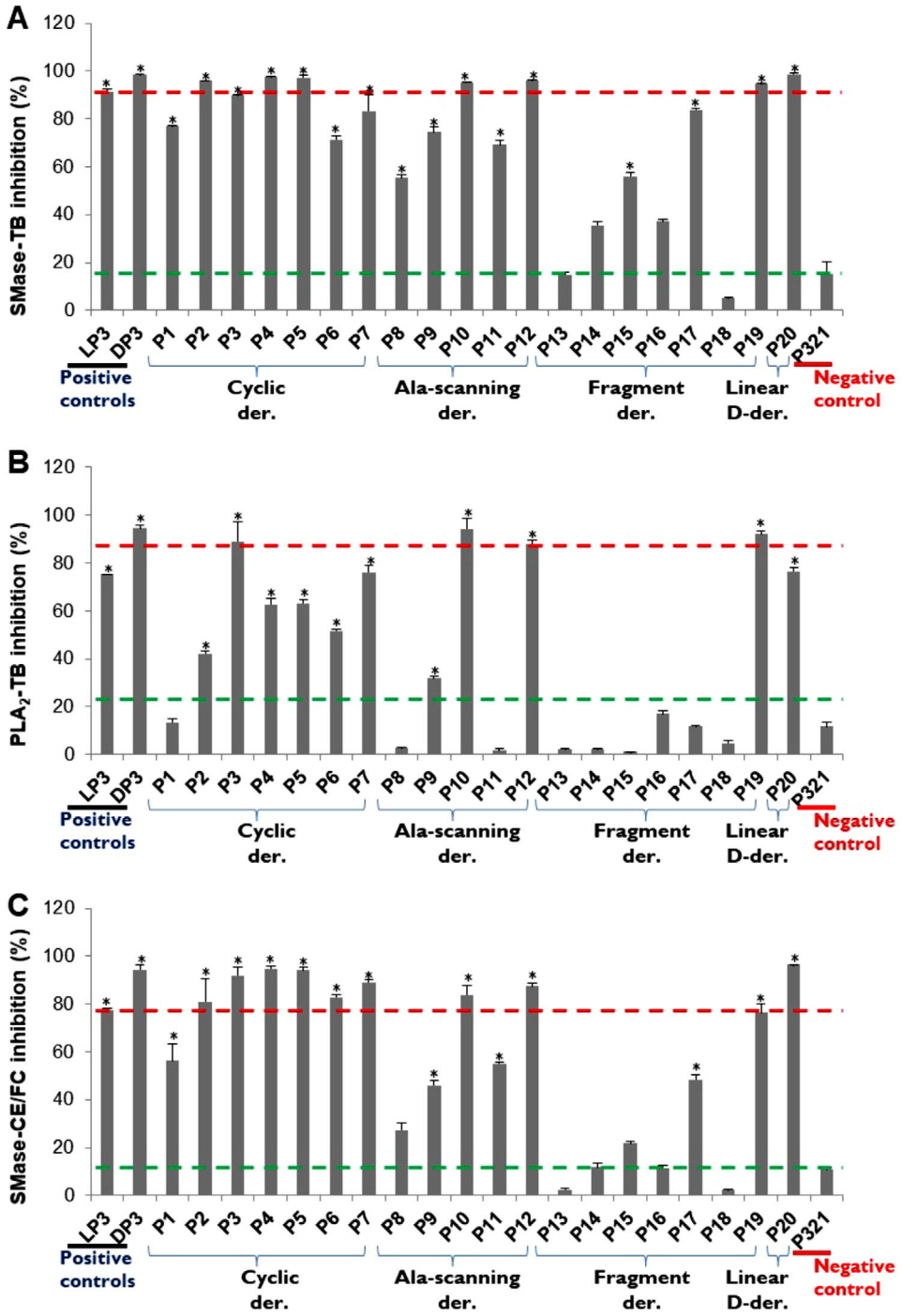

Figure 2. Inhibitory efficacy of the peptides from the first optimization round on A) SMase-TB, B) PLA_2-TB, and C) SMase-CE/FC assays. Data are presented as mean ± SD. $N = 8$ (SMase-TB), $N = 4$ (PLA_2-TB and SMase-CE/FC). *P*-values are calculated using the Mann-Whitney *U* test. $^*P < 0.01$ versus negative control. Ala: alanine, der.: derivative.

cyclic peptide analogues tested had a similar (P3) or higher (P4 and P5) efficacy than LP3. Most of the smaller fragment compounds showed lower inhibitory activity compared with the parent peptide.

We found that P17 maintained approximately the same activity as LP3 despite of its smaller size (i.e., 9 instead of 14 residues), indicating that P17 contains the essential motif to protect LDL from SMase-induced LDL aggregation. This result opens the possibility to generate a new library of compounds based on the structure of P17. Most of the LP3 alanine scanning analogues (P9–P12) showed similar or slightly lower inhibitory activity than LP3, which suggest that none of the residues Asp^7, Asn^8, Glu^{11}, and

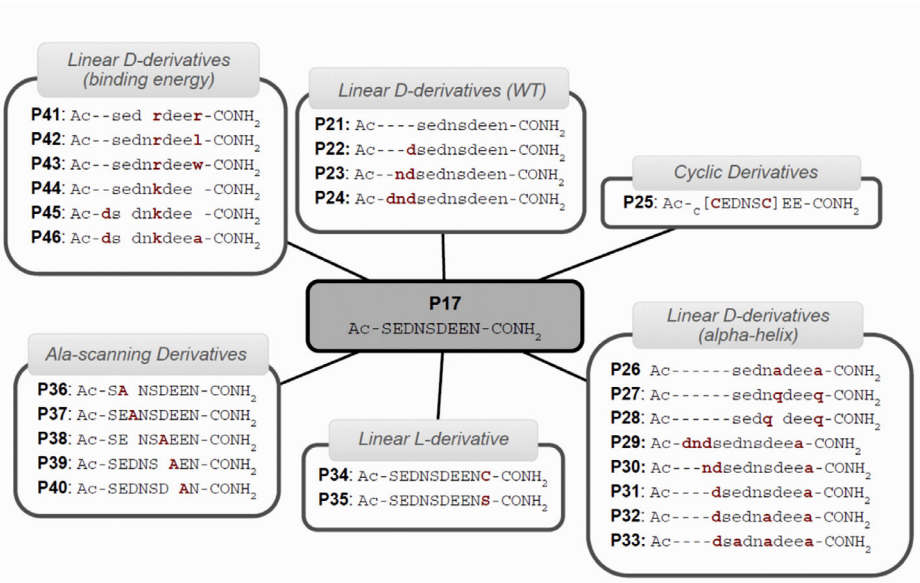

Figure 3. Schematic representation of the designed peptide groups through the development of the second-round optimization. Ala: Alanine.

Glu[12] replaced by alanine have a key role in the binding of peptide to LDL particles or that such mutations cause structural rearrangement of the peptide leading to an improvement in the binding, despite the loss of some specific intermolecular contacts. However, the replacement of Glu[6] residue by alanine led to a 30% reduction of the effects on LDL aggregation, as shown by P8 peptide.

PLA_2-TB: The inhibitory effect of the compounds on PLA_2-induced LDL aggregation is shown in Figure 2B. LP3 fragments were almost completely ineffective against PLA_2-induced LDL aggregation with the exception of P19. In contrast to P19, which maintains the same inhibitory activity to LP3 despite a smaller size, P17 was ineffective against PLA_2-induced aggregation. Interestingly, P17 and P19 differ only in one aspartate residue located at the *N*-terminal that is present in P19 but absent in P17. This suggests that this aspartate residue has a key role in the inhibitory activity against PLA_2-induced LDL aggregation. Similar to SMase-induced LDL aggregation, LP3 cyclic analogues and, in particular P3–P7, maintained a high inhibitory activity against PLA_2-induced LDL aggregation. While all the LP3 alanine-scanning analogues showed a moderate to high inhibitory activity against SMase, only P10 and P12 maintained high inhibitory activity against PLA_2 modification. These results indicate that a higher number of residues involved in intermolecular contacts are required to protect LDL against PLA_2 than against SMase. In this regard, Glu[6], Asp[7], and Glu[11] residues appear to be essential for inhibitory activity against PLA_2 but not against SMase-induced LDL aggregation.

SMase-CE/FC: The effects of the compounds on hcVSMC-cholesterol loading were evaluated by analysis of the intracellular cholesteryl ester/free cholesterol ratio using thin layer chromatography (TLC). A representative TLC is showed in Figure S3 of the Supporting Information. hcVSMC exposed to LDL (nLDL or SMase-LDL) had similar free cholesterol (FC) levels to hcVSMC unexposed to LDL, indicating that LDL did not alter FC content in these cells. Conversely, intracellular CEs detected in these cells upon exposure to LDL derived exclusively from CE supplied by LDL, as hcVSMC unexposed to LDL did not contain intracellular CE. The TLC analysis shows the high efficacy of the positive control and, in particular of DP3, to inhibit the intracellular CE/FC ratio, an index of hcVSMC-foam cell formation. Similar to the result in the SMase-TB assay, the LP3 enantiomer version had the highest efficacy in the cell-based assay.

LP3 cyclic derivatives and LP3 alanine scanning derivatives inhibited intracellular CE/FC to a similar extent to the SMase-induced LDL aggregation, which is in line with the essential LDL condition of aggregation as cause of hcVSMC cholesterol loading.[16,17,19–22]

2.3. Computational Design and Screening of Peptides from the Second-Round Optimization

2.3.1. Computational Peptide Design

The computational strategy used to design peptides in the second round of optimization resulted into 26 peptides. This second set of compounds was synthesized by means of solid-phase peptide synthesis (summarized in **Figure 3**). The peptide sequences and their characterization have been detailed in Tables S3 and S4 of the Supporting Information, respectively. Peptides were classified into the following families according to their molecular design: LP3 cyclic derivatives, LP3 alanine scanning derivatives, LP3 fragments, P17 linear D-derivatives, P17 cyclic derivatives, P17 linear L-derivatives, and P17 alanine-scanning derivatives.

P17 was one of the most promising peptides found in the first optimization round; therefore, it was chosen as the starting point for the second optimization round. P17 was optimized by applying both ligand-based and structure-based protocols similarly to the first optimization round. First, given the high inhibitory activity against LDL aggregation observed for P20 peptide (the enantiomer version of LP3 peptide) within the first optimization

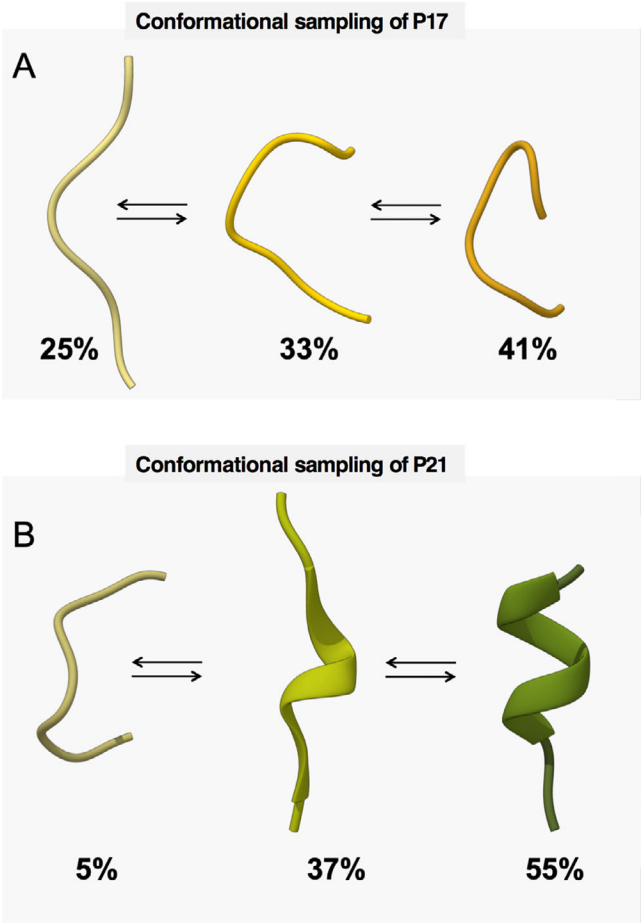

Figure 4. In silico conformational sampling of A) P17 and B) P21 peptides. Both the representative structures and the corresponding population distributions of the three most populated clusters are reported.

round, the enantiomer version of peptide P17 was taken into consideration for this second set of compounds (P21). Moreover, given the higher anti-LDL aggregation activity of P19 compared to P17, longer versions of P21 were also obtained by adding one, two, or three residues to both the *N*- and *C*-terminus P21 end, to give P22, P23, and P24. An exhaustive conformational sampling of P17 and P21 peptides was performed by MD simulations and the most populated low energy conformations were extracted. Similar to LP3, P17 peptide lacks well-defined secondary structure elements; thus, the most populated conformation was constrained leading to one cyclic analogue, namely P25. Interestingly, unlike P17, P21 only assumed quasi-helical structures, suggesting that an alpha-helix conformation could favor the interaction with ApoB-100 due to minimal conformational rearrangements upon binding and the consequent reduced entropic cost needed (**Figure 4**). On the basis of this hypothesis, the stabilization of the helix could lead to a greater decrease in energy costs and, therefore, favor the binding of the peptide to ApoB-100 protein. To favor low energy cost states, some of the P21 residues were selectively mutated into analogues with similar physicochemical properties but a higher tendency to form alpha-helix conformations (Ser to Ala and Asn to Gln).[33] This strategy led to the design of eight P21 analogues (namely, P26, P27, and P28) and five longer versions of P21 peptide (P29, P30, P31, P32, and P33). Additionally, multiple molecular docking calculations were also performed using several alternative conformations of both P17 and P20 peptides as ligand structures. MD simulations were run on the best-ranked docking poses to explore active-like conformations and design proper analogues. Based on the analysis of the specific intermolecular interactions of P17 with ApoB-100 protein, one cysteine or one serine residue was added to the P17 peptide *C*-terminal end to obtain P34 and P35 peptides, respectively. In order to confirm the essential role of several specific residues found to be deeply buried upon binding, five P17 alanine scanning analogues were generated, thus obtaining P36, P37, P38, P39, and P40 peptides.

However, four P21 analogues were generated by studying the favored orientation adopted by the peptide upon ApoB-100 protein binding. Interestingly, virtually all the negatively charged side chains were oriented to the same face of the alpha helix and, thereby, directly interacted with several positively charged residues of ApoB-100. In this context, the optimization of electrostatic interactions between the peptide and ApoB-100 could reduce the free energy and favor the final binding. For this reason, P21 peptide residues exposed to the solvent upon binding, namely, Ser^5 and Asn^9, were mutated to alanine, positively charged residues or hydrophobic residues (as negative controls), leading to the design of six new peptides (namely, P41, P42, P43, P44, P45, and P46 peptides).

2.3.2. Peptide Screening

SMase-TB: Both SMase- and PLA_2-induced assays clearly suggested that the optimization of LP3 peptide by reducing its size (P17) remained a promising approach. Nevertheless, additional modifications were needed in order to achieve similar inhibitory activity on both SMase- and PLA_2-induced LDL aggregation. In this regard the introduction of D-amino acids (second round) appeared to be a promising strategy. The effects of the compounds from the second optimization round on SMase-induced LDL aggregation are shown in **Figure** 5A. Like P20, P21 (the enantiomer version of P17) showed similar inhibitory activity compared to its parent peptide. Both the linear derivatives (P34 and P35) and the cyclic derivative (P25) had similar inhibitory effects to P17.

Unlike the results obtained on LP3 peptides, many of the P17 alanine scanning analogues, such as P36, P37, P38, P39, and P40, showed a significant decrease in the inhibitory activity compared with P17. The replacement of a single residue by alanine, led to a reduction of at least 30% in the peptide inhibitory efficacy against LDL aggregation. This clearly suggested that all these residues have a key role in the binding to LDL particles and that the deletion of their side chain leads to the loss of some specific intermolecular contacts as well as unfavorable structural rearrangements of the peptide in solution or upon ApoB-100 protein binding.

Interestingly, the attempt of enhancing P21 inhibitory effects by stabilizing the expected alpha-helix conformation (P26, P27, and P28) proved to be successful since this increased the inhibitory effects on LDL aggregation. We also observed that the

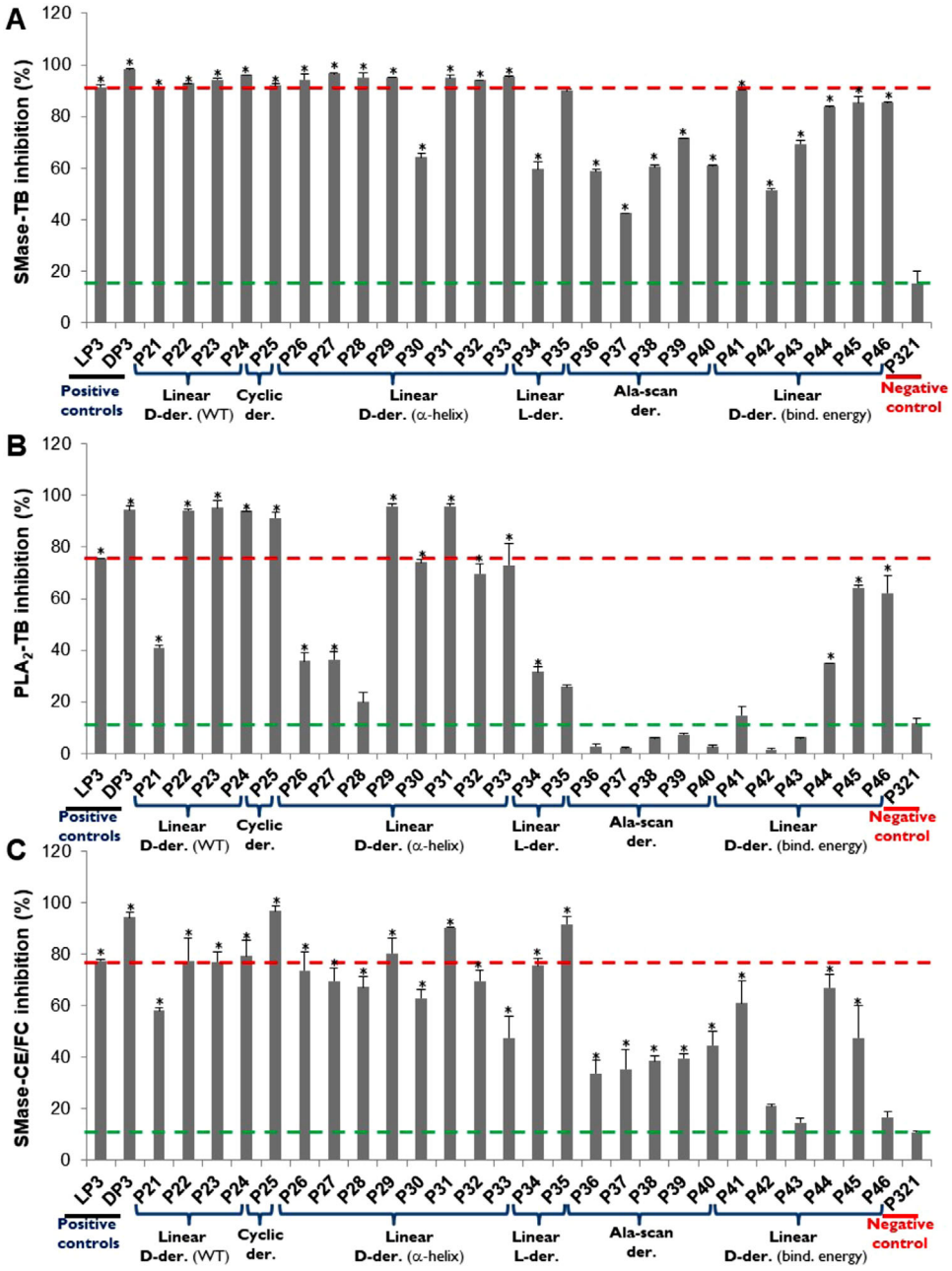

Figure 5. Inhibitory efficacy of the peptides from the second optimization round on A) SMase-TB, B) PLA_2-TB, and C) SMase-CE/FC assays. Data are presented as mean ± SD. $N = 8$ (SMase-TB), $N = 4$ (PLA_2-TB and SMase-CE/FC). *P*-values are calculated using the Mann-Whitney *U* test. $^*P < 0.01$ versus negative control. Ala: alanine, der.: derivative, scan: scanning, bind: binding, WT: wild.

addition of one, two or three residues to the original sequence do not significantly change the overall inhibitory effects (as observed in P22, P23, P24, P29, and P31) with the exception of P30, suggesting that P26 could have the optimal sequence to guarantee the highest inhibitory activity within LP3 analogues. Finally, the introduction of positively charged or hydrophobic residues led to insignificant or negative effects, as shown by P41, P42, P43, and P44 peptides. Collectively, the results from this biochemical screening shows that P21, P22, P23, P24, P26, P27, P28, P29, P31, and P41 peptides are the more promising compounds.

PLA2-TB Assay: P17 alanine-scanning analogues (P36, P37, P38, P39, and P40) were ineffective against PLA_2-induced LDL aggregation. However, some of the P17 D-amino analogues (P22, P23, P24, P29, and P31) showed maximal inhibitory activity on PLA_2-induced aggregation (Figure 5B).

Both SMase- and PLA_2-induced assays clearly pointed to P22 and P31 peptides as the most promising LP3 derivatives combining significant inhibitory activity on both SMase- and PLA_2-induced LDL aggregation with a theoretically increased plasma

Table 2. Pearson and Spearman's correlations between SMase-TB and PLA_2-TB for all peptides and peptides separated by control, first, and second optimization round compounds. SMase: Sphingomyelinase; PLA_2: phospholipase A2; TB: turbidimetry.

	Pearson	Spearman's
Total compounds (N = 46)	$r = 0.686$	$r = 0.762$
	$P < 0.001$	$P < 0.001$
Control	$r = 0.990$	$r = 1.000$
	$P = 0.092$	–
First round ($N = 20$)	$r = 0.744$	$r = 0.750$
	$P < 0.001$	$P < 0.001$
Second round ($N = 26$)	$r = 0.660$	$r = 0.718$
	$P < 0.001$	$P < 0.001$

Table 3. Pearson and Spearman's correlations between SMase-TB and SMase-CE/FC for all peptides and peptides separated by control, first, and second optimization round compounds. SMase: Sphingomyelinase; TB: turbidimetry; CE: cholesteryl esters; FC: free cholesterol.

	Pearson	Spearman's
Total compounds ($N = 46$)	$r = 0.820$	$r = 0.790$
	$P < 0.001$	$P < 0.001$
Control	$r = 0.993$	$r = 1.000$
	$P = 0.074$	–
First round ($N = 20$)	$r = 0.924$	$r = 0.906$
	$P < 0.001$	$P < 0.001$
Second round ($N = 26$)	$r = 0.620$	$r = 0.629$
	$P = 0.001$	$P = 0.001$

stability if compared with LP3 peptide because of the use of D-amino acids.

SMase-CE/FC: As shown in Figure 5C and Figure S3 (Supporting Information), most of the P17 (D-amino acids containing analogues) were highly effective for the inhibition of hcVSMC cholesterol loading. In particular, compounds P22 and P31, previously selected as the more promising LP3 analogues because of their high efficiency of inhibition of aggregation induced by both SMase and PLA_2, also showed high inhibitory effects in the intracellular cholesterol accumulation. P22 and P31 inhibited LDL aggregation and intracellular cholesterol loading to a similar extent than LP3 and substantially higher than P17 peptides.

2.4. Analysis of the Correlation between the Efficacy of the New Compounds on SMase-TB, PLA_2-TB, and SMase-CE/FC Assays

The correlations between the efficacy of compounds in the SMase-TB and PLA_2-TB assays and between the SMase-TB and SMase-CE/FC assays are shown in **Figure** 6A,B, respectively. Given the distribution of the variables, we first analyzed Spearman's correlations. However, Pearson's correlation gave similar qualitative and quantitative results for both the correlation between the efficacy of compounds in the SMase-TB and PLA_2-TB assays (**Table 2**) and between the efficacy of compounds in the SMase-TB and SMase-CE/FC assays (**Table 3**).

The strong correlation between the efficacy of the total compounds in the SMase-TB and SMase-CE/FC assays (Pearson $r = 0.820$, $P = 0.000$; Spearman's $r = 0.790$, $P = 0.000$) is in line with the key role of LDL aggregation on hcVSMC-foam cell formation, previously described by our group.[16,17,19–22] Taken together, our results from molecular, biochemical and cell-based studies point to P22 and P31 as the most promising peptides to be evaluated in vivo.

3. Discussion

Currently, the prevention of atherosclerosis and other CVDs is mainly based on lipid-lowering agents (e.g., HMG-CoA reductase and PCSK9 inhibitors) that reduce blood cholesterol levels. Although this reduction of plasma cholesterol levels undoubtedly affects the amount of cholesterol retained and accumulated in the vascular wall of the coronary vessels, it does not avoid the risk and the mortality of CVD events. Indeed, the benefit of lipid-lowering drugs, such as statin-based therapies is often not related to a sharp decrease in CVD mortality (acute myocardial infarction and angina pectoris) in atherosclerosis patients.[34] Previous studies from different groups, including ours, have highlighted the pathological relevance of blocking processes occurring locally in the arterial intima such as LDL aggregation and the uptake of aggregated LDL by smooth muscle cells.[20–22,25] We recently showed that LRP1-derived peptides, LP3, and, in particular, its retroenantiomer version (DP3) efficiently preserved LDL from SMase or PLA_2-induced LDL aggregation through the maintenance of ApoB-100 conformation.[26] We demonstrated that the protective effect of these peptides derives from their capacity to establish electrostatic interactions with a specific highly positive sequence located in the ApoB-100 *C*-terminal region. In this study, we developed LP3 peptide derivatives combining structural- and ligand-based computational designs with functional biochemical and cell-based screening systems to obtain optimized peptides with similar activity to the original peptides.

3.1. Amino Acids with D-Chirality and a Tendency to Form Alpha-Helix Conformation Promote the Formation of Peptide/ApoB-100 Stable Complexes that Are Required to Maximize Peptide Functional Activity

Peptides containing D-amino acids consistently showed far higher inhibitory activity with respect to their L-amino acid counterparts, as with P17 and P21, LP3 peptide, and P20 and P19 and P22 compounds. This effect is hypothesized to be related to a higher metabolic stability derived from their stronger resistance to proteolytic degradation as well as to a higher binding affinity to Apo-B100 protein or positive structural consequences of the binding.

Another structural feature that was observed to confer higher activity against LDL aggregation was related to the higher tendency to form alpha-helix conformations that could favor the binding of the peptide to ApoB-100 protein and increase its inhibitory activity against LDL aggregation, as was shown with P21, P26, P27, and P28.

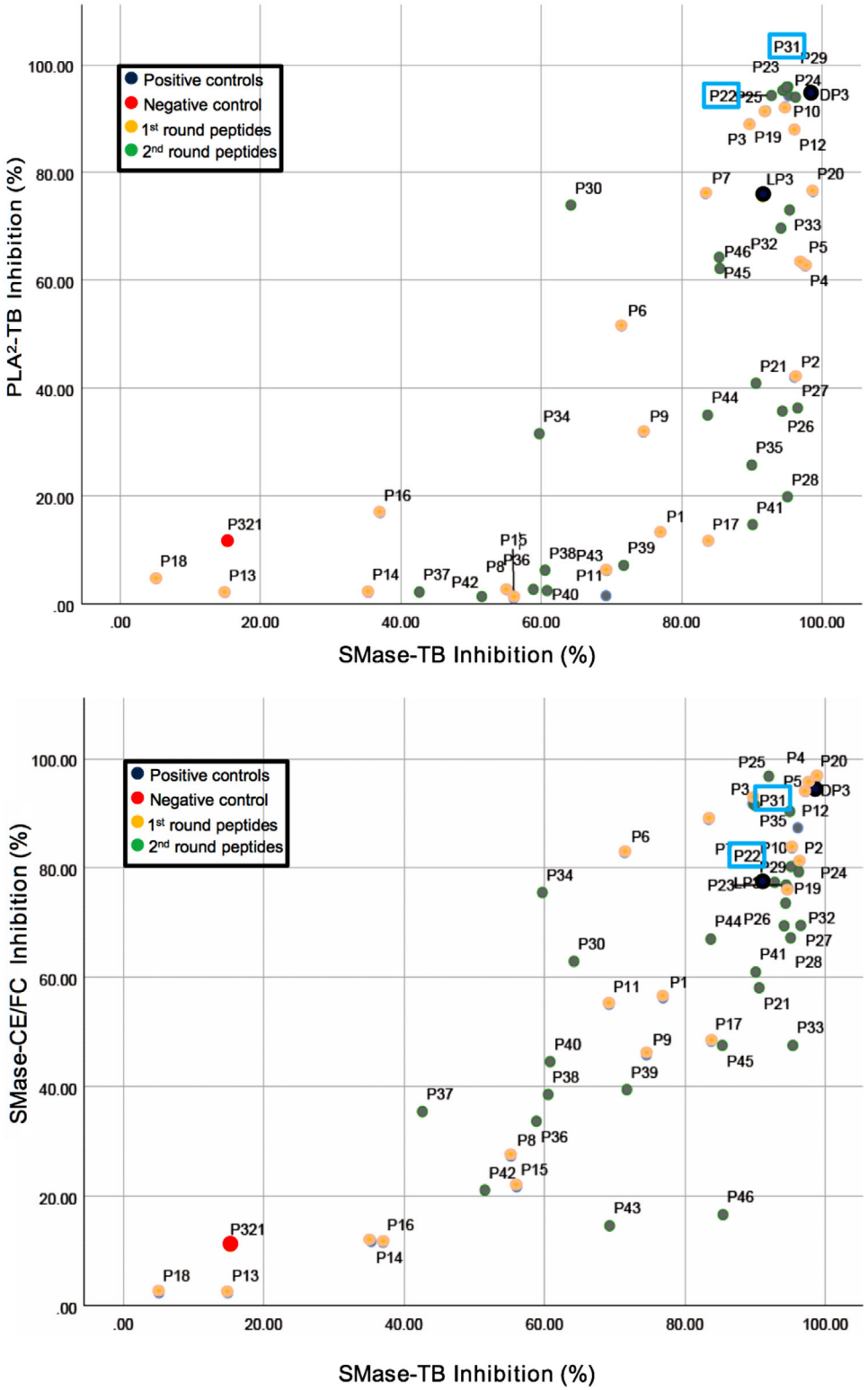

Figure 6. Graphs showing the scatterplot for the correlation A) between SMase-TB and PLA_2-TB and B) between SMase-TB and SMase-CE/FC. Blue squares label the compounds selected to perform studies in in vivo models.

3.2. Additional Molecular Peptide Optimization Requirements Are Needed to Reach Maximal Efficacy against Both SMase- and PLA_2-Induced LDL Aggregation

Despite having significant inhibitory activity on SMase-induced LDL aggregation, virtually all the 9-residue peptides, such as P17, its D-amino acid counterpart P21, and their analogues P26, P27, and P28 were found to have a very limited or null activity upon LDL aggregation induced by PLA_2. By contrast, we found that longer sequences with at least one additional residue in the *C*-terminal or the *N*-terminal end conferred higher inhibitory activity to the peptide in the PLA_2 environment. This was notable in P34 and P35, which were generated by adding a cysteine or a serine, respectively, to the *C*-terminal end of P17 sequence and in P19, which was generated by adding an aspartate to the *N*-terminal end of P17 peptide. P19, in comparison to P17, showed an inhibitory activity of more than 90% on both SMase- and PLA_2-induced LDL aggregation.

Considering the limited structural data currently available on ApoB-100 protein and the dynamic arrangement upon LDL aggregation, it is difficult to provide a comprehensive explanation of the specific structural requirements of the different peptides for the successful inhibition of LDL aggregation induced by SMase or by SMase and PLA_2. It may be reasonable to suggest that the binding of any of the active peptides to ApoB-100 protein promotes a certain conformational change on ApoB-100 itself and that it the extent of this conformational change that is related to the specific effect on LDL aggregation observed for each peptide. Additionally, shorter peptides, such as P17 or P21, may be able to induce a limited conformational change sufficient to block SMase, but not PLA_2 affecting LDL particles. Conversely, peptides composed of at least ten residues, (e.g., P19, P22 or P31) succeed in stimulating a more significant conformational change on ApoB-100 leading to the inhibition of both SMase and PLA_2-induced LDL aggregation. It is also important to note that the different requirements for the peptide to be protective against SMase and PLA_2-induced LDL aggregation are related to the different locations of SM (the substrate of SMase) and PC (the substrate of PLA_2) on the LDL surface.[35] SM is protected by these peptides against phospholipolysis as it is part of cholesterol-enriched domains, whose structure, preserved through the formation of peptide-ApoB-100 complexes, modulates SM lipolysis. By contrast, PC is located outside of these cholesterol-enriched domains, and, therefore, is not protected by this mechanism. Thus, the preservation of LDL against PLA_2-induced LDL aggregation requires longer peptides that ensure ApoB-100 conformation in conditions of extreme lipolysis.

3.3. Targeting LDL Aggregation as a Therapeutic Strategy to Inhibit hcVSMC-Cholesterol Loading

This study demonstrated a strong correlation between the inhibitory activity of peptides on SMase-induced LDL aggregation and hcVSMC-cholesterol loading. These results are in line with the pivotal role of agLDL on foam cell formation from smooth muscle cells.[16–19] AgLDL is a key contributor of extracellular cholesterol plaque burden since extracellular matrix proteoglycans and proteolytic enzymes of the arterial intima strongly promote agLDL formation.[9–12] In addition, targeting foam cell formation confers atheroprotection.[36,37] AgLDL also upregulates its own receptor, LRP1, initiating a potent cycle that promotes foam cell formation and increases plaque cholesterol burden.[19,24,25] At a clinical level plaque burden determines the rapid progression of asyntomatic to syntomatic plaques, as reported in a prospective observational study performed in 1.345 patients from 13 centers and seven countries.[38] We previously reported that aggregated LDL induces the production and secretion of tissue factor, the main initiator of thrombosis, by human coronary VSMC.[21,22] Recent studies report that susceptibility of LDL to aggregate is associated with future coronary artery disease events.[39] We recently reported that circulating levels of soluble LRP1 (sLRP1) predict future cardiac events at ten years in the cohort REGICOR.[40] Together, these studies highlight the potential relevance and clinical interest of these compounds in the treatment of atherosclerosis and in the management of cardiovascular disease.

3.4. Essential Features of Optimized Peptides Selected to be Assayed in Preclinical Models of Atherosclerosis

On the basis of both two computational strategies, namely, structure- and ligand-based drug design, 46 compounds were designed according to the minimal energy status of the complex and maximal stability. This facilitated peptide cycling with the final aim of finding the minimal motif within LP3 peptide amino acid sequence able to inhibit both SMase- and PLA_2-induced LDL aggregation. A key structural feature that confers high activity against LDL aggregation is the tendency to form alpha-helix conformations that favor peptide/ApoB-100 protein complex formation and increase its inhibitory activity against LDL aggregation, as shown with P21, P26, P27, and P28.

However, peptides composed of at least ten residues (e.g., P19, P22, or P31) succeed in augmenting a more significant conformational change on ApoB-100 leading to the inhibition of both SMase- and PLA_2-induced LDL aggregation.

Taking into account all these considerations, P22 and P31, which are P17-derived D-amino acid analogues are highly efficient in inhibiting both SMase- and PLA_2-induced LDL aggregation. These enzymes are extremely active in the intimal extracellular matrix and these compounds are relatively small and expected to be highly stable against proteases. In this context, compounds P22 and P31 are highly promising to be tested in preclinical models of atherosclerosis.

3.5. Clinical Implications

Although statin-based therapy is generally well tolerated and highly effective in lowering blood cholesterol levels, it can be associated with various adverse events (e.g., intolerance, myalgia, myopathy, rhabdomyolysis, and diabetes mellitus)[41] and with an increased incidence of diabetes.[42] Indeed, as diabetic patients suffer a high incidence of atherosclerosis and cardiovascular pathology, the development of innovative drugs for the treatment of atherosclerosis in these patients, or those with high susceptibility of diabetes development, is becoming of vital importance. In this context, inhibiting vascular cholesterol

accumulation by modulating not only LDL aggregation but also aggregated LDL internalization by vascular cells may be a promising therapeutic strategy in the treatment of cardiovascular disease.

4. Experimental Section

Molecular Modeling—In Silico Conformational Sampling: The in silico conformational sampling of LP3 peptide included a conjugate gradient minimization, an equilibration, and 100 ns long implicit solvent MD simulation using NAMD simulation package.[43] Thus, as the first preparation step, an LP3 3D structure was created from scratch and parameterized using AmberTool16 Leap module and ff12 AMBER force field.[44] Then, a 1000-cycle long minimization was performed applying harmonic restraints to all nonhydrogen atoms with a force constant of 5 kcal mol^{-1} $Å^{-2}$ in order to remove initial intermolecular clashes. A 200 ps long equilibration was run gradually heating the system to 56.85 °C and applying harmonic restraints with the same force constant as in the minimization but only to the backbone atoms. During equilibration, the integration time step was set to 2 fs and the nonbonding cut off distance to 12 Å. Then, an unrestrained replica exchange molecular dynamics simulation in implicit water was run consisting of 16 independent 100 ns long trajectories (replicas) performed simultaneously at temperatures ranging from 26.85 to 339.85 °C. Finally, 10 000 snapshots were extracted from the 300 K trajectory and were consequently clustered using the single linkage method by the cpptraj AMBER tool. A representative structure of each cluster was selected and conformationally constrained by mutating two specific residues to cysteine in order to obtain LP3 cyclic derivatives in the first optimization round, via intramolecular disulphide bridge formation. The same strategy was used to perform the conformational sampling of P17 and P21 compounds within the second optimization round.

Molecular Modeling—I ApoB-100 Molecular Docking: The structural model of ApoB-100 in complex with LP3 peptide was built by rigid body molecular docking simulation using the corresponding peptide conformers described above, as ligands, and ten different ab initio models of ApoB-100 LDL receptor binding domain, generated as previously described,[26] as receptors.

Starting from each ApoB-100 protein structure and LP3 peptide conformer previously obtained, different independent docking simulations were performed using SMINA, an energy minimization optimized fork of the AutoDock Vina docking program.[45] All the ligands and the receptor structures were converted into input files suitable for SMINA using prepare_ligand4.py and prepare_receptor4.py scripts provided by AutoDock Tools.[46] A cuboid grid box of roughly $60 \times 60 \times 60$ size with a grid space of 0.375 Å was adjusted around Apo-B100 ^{3227}IKFDKYKAEK^{3236} region, assumed to be responsible for LP3 peptide recognition according to previous studies.[26] Exhaustiveness, number of modes and energy range were set to 32, 100, and 50, respectively.

Once all the docking simulations were run, the lowest energy-docking pose of each conformer in complex with ApoB-100 protein was selected and submitted to a postdocking MD-based structural refinement. Thus, each docking model underwent a conjugate gradient minimization, equilibration, and 3 ns long implicit solvent MD simulation, using NAMD simulation package. As in the first preparation step, the overall protonation and parameterization of the system was performed using the Leap module of AmberTool16 and ff12 AMBER force field. A 1.000-cycle long minimization step was performed applying harmonic restraints to all backbone atoms of the system (both receptor and ligand) with a force constant of 5 kcal mol^{-1} $Å^{-2}$. Then, a 200 ps long equilibration step was performed gradually heating the system to 300 K and applying harmonic restraints to the backbone atoms of the protein and the ligand with a force constant of 5 and 2 kcal mol^{-1} $Å^{-2}$, respectively. Finally, a 3 ns long MD simulation was performed applying harmonic restraints only to the backbone atoms of the receptor protein with a force constant of 2 kcal mol^{-1} $Å^{-2}$. In all the simulations, SHAKE[47] was applied to restrain all bonds to hydrogen atoms while a 2 fs simulation time step and a 12 Å cut off distance for long-range interaction were set.

Finally, the binding stability of each conformer was assessed by computing its average root-mean-square deviation ($LigRMSD_{avg}$) along the last 1.5 ns of the trajectory using ICM Browser Pro software (Molsoft, LLC, La Jolla, CA).[48] Conformers with $LigRMSD_{avg}$ values lower than 2 Å were predicted as stable binders, close to the peptide active state and thus selected to be conformationally restrained, when possible, by mutating two specific residues to cysteine in order to obtain LP3 cycled derivatives. A similar protocol was applied to obtain derivatives of the P17 compound, one of the most promising LP3 derivatives obtained in the first optimization round, within the second optimization round. As no feasible cycled derivatives were produced during the second round, linear derivatives were generated from the selected conformers based on the visual inspection of the specific intermolecular interactions of the docking partners.

Additionally, the most frequently buried residues upon binding, in terms of accessible solvent area (ASA) within all the selected conformers were identified and used to design additional LP3 and P17 linear derivatives. The ASA value was calculated by ICM browser software.[48]

Peptide Synthesis: All the peptides were synthesized by Iproteos S.L (Barcelona, Spain) by means of solid-phase peptide synthesis following a 9-fluorenylmethoxycarbonyl/*tert*-butyl (Fmoc/*t*Bu) strategy. Syntheses were performed manually on a 100 μmol scale per peptide using Rink amide ChemMatrix resin. Peptide elongation and other solid-phase manipulations were done manually in polypropylene syringes, each fitted with a polyethylene porous disk. Solvents and soluble reagents were removed by suction. Washings between synthetic steps were done with dimethylformamide and dichloromethane using 5 mL of solvents per gram resin each time. N^{α}-Fmoc-protected amino acids (four equivalents) were coupled using 2-(1H-benzotriazole-1-yl)-1,1,3,3-tetramethyluronium (four equivalents), and *N*,*N*-diisopropylethylamine (eight equivalents). The extent of the reaction was monitored using the Kaiser test. During couplings, the mixture was allowed to react with intermittent manual stirring. The Fmoc group was removed by treating the resin with 20% piperidine in DMF (3 mL g^{-1} resin). The peptides were cleaved from the resin using a mixture of trifluoroacetic acid, triisopropylsilane, and water (95:2.5:2.5). The crude products obtained were purified in reverse phase using a semiprep HPLC instrument equipped with a C18 column. The purity and identity of the synthesized peptides were assessed by HPLC, HPLC-MS, and MALDI-TOF analysis.

In silico designed and synthesized compounds (N = 46) were evaluated in a double screening system: The efficacy of the compounds to inhibit LDL aggregation was first monitored by turbidimetry. The turbidimetry assay has been optimized for screening by 1) using the enzymatic (SMase or PLA_2) induction of LDL aggregation and 2) using LDL from a unique normolipemic pool (Figure S1, Supporting Information).

Biochemical/Cell-Based Screening Assays for Peptide Efficacy—LDL Isolation and Purification: Human LDL ($d_{1.019}$–$d_{1.063}$ g mL^{-1}) was obtained from pooled normolipemic human plasma by sequential ultracentrifugation in a KBr density gradient. Briefly, very-low density lipoproteins (VLDLs) were first discarded after spinning plasma at 50 000 *g* for 18 h at 4 °C using a fixed-angle rotor (50.2 Ti, Beckman) mounted on an Optima L-100 XP ultracentrifuge (Beckman). Subsequently, VLDL-free plasma was layered with 1.063 g mL^{-1} KBr solution and centrifuged at 50 000 *g* for 18 h at 4 °C. LDLs were dialyzed against 0.02 M Trizma, 0.15 M NaCl, 1×10^{-3} M EDTA, pH 7.5 for 18 h and then against normal saline for 2 h at 4 °C. Finally, isolated LDLs were filter-sterilized (0.22 μm Millex-GV filter unit, Millipore). Protein concentration was determined using the BCA protein assay (Thermo Scientific) and the cholesterol concentration was determined with a commercial kit (IL test Cholesterol, Izasa).

Biochemical/Cell-Based Screening Assays for Peptide Efficacy—Exposure of LDL to Sphingomyelinase (SMase) or Phospholipase A2 (PLA_2) in the Presence and Absence of Peptides under Strictly Controlled Conditions: Human LDL (1.44 mg mL^{-1}) were incubated with 40 U L^{-1} of *Bacillus cereus* SMase (Sigma-Aldrich, Schnelldorf, Germany) or with 50 μg L^{-1} of type II secretory PLA_2 from honey bee venom (Sigma-Aldrich, Schnelldorf, Germany) in 20×10^{-3} M Tris buffer (pH 7.0) containing 150×10^{-3} M NaCl, 2 ×

10^{-3} M $CaCl_2$, and 2×10^{-3} M $MgCl_2$ at 37 °C. LDL incubation with SMase (24 h) or PLA_2 (36 h) was performed in absence or presence of peptides at peptide concentrations of 10×10^{-6} M (peptide/ApoB-100 ratio: 5/1) on the basis of the results obtained in dose- and time-course previous experiments.[26] LDL lipolysis was stopped by addition of EDTA (final concentration 10×10^{-3} M).

Biochemical/Cell-Based Screening Assays for Peptide Efficacy—Quantification of the Inhibitory Efficacy of Each Compound against LDL Aggregation Induced by SMase or PLA_2: The efficiency of peptides to inhibit LDL aggregation induced by SMase or PLA_2 was estimated by turbidimetry measuring the absorbance at a wavelength of 405 nm. The inhibitory activity was calculated according to Equation (1)

$$\text{Inhibition activity} = [1 - (a - b/c - b)] * 100 \quad \text{(I)}$$

wherein

a corresponds to the absorbance value in the presence of nLDL particles, LDL aggregating enzyme (i.e., SMase or PLA_2) and test compound,
b corresponds to the absorbance value in the presence of only nLDL particles, and
c corresponds to the absorbance value in the presence of nLDL particles and LDL aggregating enzyme (i.e., SMase or PLA_2).

Biochemical/Cell-Based Screening Assays for Peptide Efficacy—Cell-Based Screening Assay: The efficacy of the peptides to inhibit LDL-induced intracellular cholesteryl ester accumulation was monitored by determination of intracellular CE/FC ratio. The cellular assay has been optimized for screening by 1) using the cells from a unique batch through all experiments and 2) testing LDL aggregation degree before adding LDL to the cell culture.

Biochemical/Cell-Based Screening Assays for Peptide Efficacy—Quiescent hcVSMCs: Cells of a single lot batch (61 646 600) were obtained from ATCC (ATCC-PCS-100-021) to prevent variability derived from cell origin. Quiescence was induced by maintaining the cell culture for 24 h in a medium with 0.2% foetal calf serum or for 48 h in a medium with 0.4% serum at 37 °C and 5% CO_2. Serum-deprived cells between passages 4 and 8 were used for experiments. Cells at these passages appeared as a relatively homogeneous population with a hill-and-valley confluence pattern. Cell monolayers were grown in vascular cell basal medium (ATCC-PCS-100-030) supplemented with vascular smooth muscle growth kit components (ATCC-PCS-100-042). Quiescent cells were exposed for 2 h to LDL previously treated with SMase for 18 h in the presence or absence of peptides at a concentration of 10×10^{-6} M. The degree of aggregation of the added LDL was assessed by turbidimetry measurements before the incubation with the cells (Figure S4, Supporting Information). Cells were not exposed to PLA_2-treated LDL due to the high cytotoxicity of PLA_2. Cells were collected for lipid extraction followed by neutral intracellular lipid partitioning through thin layer chromatography and lipid band analysis and quantification.

Biochemical/Cell-Based Screening Assays for Peptide Efficacy—Determination of Intracellular Cholesteryl Ester/Free Cholesterol Ratio: Following the lipoprotein incubation period, hcVSMCs were washed exhaustively: twice with phosphate buffered saline (PBS), twice with PBS supplemented with 1% bovine serum albumin (BSA), and once with PBS supplemented with both 1% BSA and 100 U mL^{-1} heparin); cells were then harvested into 1 mL of 0.15 M NaOH. Lipids were extracted using the Bligh and Dyer method with minor modifications.[17,19] The lipid extract was dissolved in dichloromethane, applied to silica gel plates, and separated by thin layer chromatography. Cholesterol and cholesterol palmitate were run as standards of free and cholesteryl ester, respectively. A primary solvent combination of heptane/diethylether/acetic acid (74:21:4, v/v/v) was used as chromatographic mobile phase followed by heptane alone. After lipid separation, the plates were dried and stained as previously reported.[24] Finally, the spots corresponding to CE and FC were measured by densitometry against the standard curve using a GS-800 Calibrated Densitometer (Bio-Rad).

Biochemical/Cell-Based Screening Assays for Peptide Efficacy—Calculation of the Inhibitory Efficacy of Each Compound against hcVSMC-Cholesterol Loading: hcVSMC exposed to LDL (nLDL or SMase-LDL) showed similar FC levels compared to hVSMC not exposed to LDL, indicating that LDL did not alter FC content in these cells. Conversely, intracellular CEs detected in these cells upon exposure to LDL derives exclusively from CE supplied by LDL, as hcVSMC unexposed to LDL did not have intracellular CEs. The inhibitory effect of the novel compounds on the intracellular cholesterol accumulation was analyzed in terms of decrease in the ratio of intracellular CE and FC content of hcVSMC exposed to LDL and SMase-LDL.

The efficacy of each peptide to decrease the ratio of intracellular CE and FC content of hcVSMC exposed to LDL and SMase-LDL was calculated according to Equation (2)

$$\text{Efficacy} = [1 - (a - b/c - b)] * 100 \quad (2)$$

wherein

a corresponds to the CE/FC ratio in hcVSMC exposed to SMase-LDL and in the presence of the test compound,
b corresponds to the CE/FC ratio in hcVSMC exposed to nLDL in the absence of the test compound, and
c corresponds to the CE/FC ratio in hcVSMC exposed to SMase-LDL in the absence of the test compound.

Statistical Analysis: Data were described as the mean ± standard deviation (SD). Comparisons among groups were performed using Mann-Whitney *U* test. Correlation between continuous variables was analyzed using both Pearson's linear correlation coefficient and the Spearman's rho coefficient. Correlation was plotted using a scatterplot, identifying the values of each round. The interassay CV was calculated as the average coefficient of variation form plate control means and the intra-assay CV was calculated as the average coefficient of variation between duplicates. The Z-factor was calculated as previously described.[27] The two-tailed significance level was set at <0.05. The statistical software package IBM-SPSS (V25) was used for statistical analyses.

Supporting Information

Supporting Information is available from the Wiley Online Library or from the author.

Acknowledgements

A.B.-A. and C.P. contributed equally to this work. The authors thank Dr. Ignasi Gich, Professor of Clinical Pharmacology and Therapeutics and Researcher of Sant Pau Biomedical Research Institute (IIB-SantPau) and CIBER Epidemiología y Salud Pública (CIBERESP), for this help in statistical analysis and graph representations. The Ministry of Science and Innovation of Spain, in the framework of the State Plan of Scientific and Technical Innovation Investigation 2013–2016, awarded funding to the project "DEVELOPMENT OF AN INNOVATIVE THERAPY FOR THE TREATMENT OF THE ATHEROSCLEROSIS THROUGH INHIBITION OF CHOLESTEROL VASCULAR ACCUMULATION" led by IPROTEOS SL with File No. RTC-2016-5078-1. Support was also received from the Fundació MARATÓ TV3 Project 201521-10 (to VLl-C), and FIS PI18/01584 (to VLl-C) from the Instituto de Salud Carlos III (ISCIII) and cofinanced with ERDFs. Support was also received from Ministerio de Economía y Competitividad to DdG-C (IJCI-2016-29393). CIBER Enfermedades Cardiovasculares (CIBERCV; CB16/1100403 (DdG-C, VLl-C) are projects run by the Instituto de Salud Carlos III (ISCIII). The authors also acknowledge the support from "Secretaria d'Universitats i Recerca del Departament d'Economia I Coneixement de la Generalitat de Catalunya" (2017SGR946 to VLl-C).

Conflict of Interest

R.P., C.P., and T.T. are employees of Iproteos SL. T.T. is cofounder of Iproteos SL and member of its board of directors. Some of the results presented in this manuscript were previously described in the European Patent Application EP19382335.8

Keywords

aggregated LDL, ApoB-100, atherosclerosis, LRP1-derived peptides

Received: February 26, 2020
Revised: April 9, 2020
Published online: May 20, 2020

[1] W. P. Castelli, K. Anderson, P. W. F. Wilson, D. Levy, *Ann. Epidemiol.* **1992**, *2*, 23.
[2] T. Gordon, W. P. Castelli, M. C. Hjortland, W. B. Kannel, T. R. Dawber, *Am. J. Med.* **1977**, *62*, 707.
[3] H.-J. Guretzki, K.-D. Gerbitz, B. Olgemöller, E. Schleicher, *Atherosclerosis* **1994**, *107*, 15.
[4] M. Aikawa, P. Libby, *Cardiovasc. Pathol.* **2004**, *13*, 125.
[5] A. Mauriello, G. M. Sangiorgi, R. Virmani, S. Trimarchi, D. R. Holmes Jr., F. D. Kolodgie, D. G. Piepgras, G. Piperno, D. Liotti, J. Narula, P. Righini, A. Ippoliti, L. G. Spagnoli, *Atherosclerosis* **2010**, *208*, 572.
[6] R. Puri, S. E. Nissen, M. Shao, M. B. Elshazly, Y. Kataoka, S. R. Kapadia, E. M. Tuzcu, S. J. Nicholls, *Arterioscler. Thromb. Vasc. Biol.* **2016**, *36*, 2220.
[7] K. Öörni, P. Posio, M. Ala-Korpela, M. Jauhiainen, P. T. Kovanen, *Arterioscler. Thromb. Vasc. Biol.* **2005**, *25*, 1678.
[8] K. Oörni, M. O. Pentikäinen, M. Ala-Korpela, P. T. Kovanen, *J. Lipid Res.* **2000**, *41*, 1703.
[9] S. Marathe, S. L. Schissel, M. J. Yellin, N. Beatini, R. Mintzer, K. J. Williams, I. Tabas, *J. Biol. Chem.* **1998**, *273*, 4081.
[10] S. L. Schissel, J. Tweedie-Hardman, J. H. Rapp, G. Graham, K. J. Williams, I. Tabas, *J. Clin. Invest.* **1996**, *98*, 1455.
[11] M. Aviram, I. Maor, *Biochem. Biophys. Res. Commun.* **1992**, *185*, 465.
[12] K. Öörni, J. K. Hakala, A. Annila, M. Ala-Korpela, P. T. Kovanen, *J. Biol. Chem.* **1998**, *273*, 29127.
[13] M. W. Von Ballmoos, D. Dubler, M. Mirlacher, G. Cathomas, J. Muser, B. C. Biedermann, *Arterioscler. Thromb. Vasc. Biol.* **2006**, *26*, 359.
[14] J. C. Khoo, E. Miller, P. McLoughlin, D. Steinberg, *Arterioscler. Thromb. Vasc. Biol.* **1988**, *8*, 348.
[15] H. S. Kruth, *Curr. Opin. Lipidol.* **2002**, *13*, 483.
[16] P. Vijayagopal, D. L. Glancy, *Arterioscler. Thromb. Vasc. Biol.* **1996**, *16*, 1112.
[17] T. Dissmore, C. I. Seye, D. M. Medeiros, G. A. Weisman, B. Bradford, L. Mamedova, *Atherosclerosis* **2016**, *252*, 128.
[18] V. Llorente-Cortés, M. Otero-Viñas, E. Hurt-Camejo, J. Martínez-González, L. Badimon, *Arterioscler. Thromb. Vasc. Biol.* **2002**, *22*, 387.
[19] V. Llorente-Cortés, M. Otero-Viñas, S. Sánchez, C. Rodríguez, L. Badimon, *Circulation* **2002**, *106*, 3104.
[20] V. Llorente-Cortés, P. Costales, J. Bernués, S. Camino-Lopez, L. Badimon, *J. Mol. Biol.* **2006**, *359*, 950.
[21] V. Llorente-Cortés, M. Otero-Viñas, S. Camino-López, O. Llampayas, L. Badimon, *Circulation* **2004**, *110*, 452.
[22] S. Camino-López, L. Badimon, A. GonzáLez, D. Canals, E. Peña, V. Llorente-Cortés, *J. Thromb. Haemost.* **2009**, *7*, 2137.
[23] S. Allahverdian, A. C. Chehroudi, B. M. McManus, T. Abraham, G. A. Francis, *Circulation* **2014**, *129*, 1551.
[24] P. Costales, P. Fuentes-Prior, J. Castellano, E. Revuelta-Lopez, M. Á. Corral-Rodríguez, L. Nasarre, L. Badimon, V. Llorente-Cortes, *J. Biol. Chem.* **2015**, *290*, 14852.
[25] O. Bornachea, A. Benitez-Amaro, A. Vea, L. Nasarre, D. de Gonzalo-Calvo, J. C. Escola-Gil, L. Cedo, A. Iborra, L. Martinez-Martinez, C. Juarez, J. A. Camara, C. Espinet, M. Borrell-Pages, L. Badimon, J. Castell, V. Llorente-Cortés, *Theranostics* **2020**, *10*, 3263.
[26] A. Benitez-Amaro, C. Pallara, L. Nasarre, A. Rivas-Urbina, S. Benitez, A. Vea, O. Bornachea, D. de Gonzalo-Calvo, G. Serra-Mir, S. Villegas, R. Prades, J. L. Sanchez-Quesada, C. Chiva, E. Sabido, T. Tarragó, V. Llorente-Cortés, *Biochim. Biophys. Acta – Biomembr.* **2019**, *1861*, 1302.
[27] J.-H. Zhang, T. D. Y. Chung, K. R. Oldenburg, *J. Biomol. Screen.* **1999**, *4*, 67.
[28] F. B. Straub, G. Szabolcsi, *Molecular Biology: Problems and Perspectives*, Nauka, Moscow **1964**, Ch. 182.
[29] P. Závodszky, L. V Abaturov, Y. M. Varshavsky, *Acta. Biochim. Biophys. Acad. Sci. Hung.* **1966**, *1*, 389.
[30] D. E. Koshland, *Proc. Natl. Acad. Sci. USA* **1958**, *44*, 98.
[31] T. Clackson, J. A. Wells, *Science* **1995**, *267*, 383.
[32] R. Prades, B. Oller-Salvia, S. M. Schwarzmaier, J. Selva, M. Moros, M. Balbi, V. Grazú, J. M. De La Fuente, G. Egea, N. Plesnila, M. Teixidõ, E. Giralt, *Angew. Chem., Int. Ed.* **2015**, *54*, 3967.
[33] C. Nick Pace, J. Martin Scholtz, *Biophys. J.* **1998**, *75*, 422.
[34] R. DuBroff, *World. J. Cardiol.* **2015**, *7*, 404.
[35] T. Hevonoja, M. O. Pentikäinen, M. T. Hyvönen, P. T. Kovanen, M. Ala-Korpela, *Biochim. Biophys. Acta – Mol. Cell. Biol. Lipids* **2000**, *1488*, 189.
[36] S. H. Son, Y. H. Goo, M. Choi, P. K. Saha, K. Oka, L. C. Chan, A. Paul, *Cardiovasc. Res.* **2016**, *109*, 294.
[37] A. Maier, H. Wu, N. Cordasic, P. Oefner, B. Dietel, C. Thiele, A. Weidemann, K. U. Eckardt, C. Warnecke, *FASEB. J.* **2017**, *31*, 4971.
[38] S. E. Lee, J. M. Sung, A. Rizvi, F. Y. Lin, A. Kumar, M. Hadamitzky, Y. J. Kim, E. Conte, D. Andreini, G. Pontone, M. J. Budoff, I. Gottlieb, B. K. Lee, E. J. Chun, F. Cademartiri, E. Maffei, H. Marques, J. A. Leipsic, S. Shin, J. Hyun Choi, K. Chinnaiyan, G. Raff, R. Virmani, H. Samady, P. H. Stone, D. S. Berman, J. Narula, L. J. Shaw, J. J. Bax, J. K. Min, H. J. Chang, *Circ. Cardiovasc. Imaging* **2018**, *11*, e007562.
[39] M. Ruuth, S. D. Nguyen, T. Vihervaara, M. Hilvo, T. D. Laajala, P. K. Kondadi, A. Gisterå, H. Lähteenmäki, T. Kittilä, J. Huusko, M. Uusitupa, U. Schwab, M. J. Savolainen, J. Sinisalo, M.-L. Lokki, M. S. Nieminen, A. Jula, M. Perola, S. Ylä-Herttula, L. Rudel, A. Öörni, M. Baumann, A. Baruch, R. Laaksonen, D. F. J. Ketelhuth, T. Aittokallio, M. Jauhiainen, R. Käkelä, J. Borén, K. J. Williams, P. T. Kovanen, K. Öörni, *Eur. Heart J.* **2018**, *39*, 2562.
[40] D. de Gonzalo-Calvo, R. Elosua, A. Vea, I. Subirana, S. Sayols-Baixeras, J. Marrugat, V. Llorente-Cortés, *Atherosclerosis* **2019**, *287*, 93.
[41] P. P. Toth, A. M. Patti, R. V. Giglio, D. Nikolic, G. Castellino, M. Rizzo, M. Banach, *Am. J. Cardiovasc. Drugs* **2018**, *18*, 157.
[42] M. Barylski, D. Nikolic, M. Banach, P. Toth, G. Montalto, M. Rizzo, *Curr. Pharm. Des.* **2014**, *20*, 3657.
[43] J. C. Phillips, R. Braun, W. Wang, J. Gumbart, E. Tajkhorshid, E. Villa, C. Chipot, R. D. Skeel, L. Kalé, K. Schulten, *J. Comput. Chem.* **2005**, *26*, 1781.
[44] D. A. Case, T. E. Cheatham III, T. Darden, H. Gohlke, R. Luo, K. M. Merz Jr., A. Onufriev, C. Simmerling, B. Wang, R. J. Woods, *J. Comput. Chem.* **2005**, *26*, 1668.
[45] O. Trott, A. J. Olson, *J. Comput. Chem.* **2010**, *31*, 455.
[46] G. M. Morris, W. Huey, W. Lindstrom, M. F. Sanner, R. K. Belew, D. S. Goodsell, A. J. Olson, A. J. Olson, *J. Comput. Chem.* **2009**, *30*, 2782.
[47] J.-P. Ryckaert, G. Ciccotti, H. J. C. Berendsen, *J. Comput. Phys.* **1977**, *23*, 327.
[48] R. Abagyan, W. H. Lee, E. Raush, L. Budagyan, M. Totrov, M. Sundstrom, B. D. Marsden, *Trends. Biochem. Sci.* **2006**, *31*, 76.